

Solving larger Travelling Salesman Problem networks with a penalty-free Variational Quantum Algorithm

Daniel Goldsmith ^{*1, 2}, Xing Liang ^{†1}, Dimitrios Makris¹, and Hongwei Wu³

¹Faculty of Engineering, Computing and the Environment,
University of Kingston, London, KT1 2EE

²Digital Catapult, 101 Euston Road, London, NW1 2RA

³Centre for Engineering Research, University of Hertfordshire,
Hatfield, AL10 9AB

November 2025

Abstract

The Travelling Salesman Problem (TSP) is a well-known NP-Hard combinatorial optimisation problem, with industrial use cases such as last-mile delivery. Although TSP has been studied extensively on quantum computers, it is rare to find quantum solutions of TSP network with more than a dozen locations. In this paper, we present high quality solutions in noise-free Qiskit simulations of networks with up to twelve locations using a hybrid penalty-free, circuit-model, Variational Quantum Algorithm (VQA). Noisy qubits are also simulated. To our knowledge, this is the first successful VQA simulation of a twelve-location TSP on circuit-model devices. Multiple encoding strategies, including factorial, non-factorial, and Gray encoding are evaluated.

^{*}Corresponding Author: D.Goldsmith@kingston.ac.uk

[†]Principal Corresponding Author: X.Liang@kingston.ac.uk

Our formulation scales as $\mathcal{O}(n \log_2(n))$ qubits, requiring only 29 qubits for twelve locations, compared with over 100 qubits for conventional approaches scaling as $\mathcal{O}(n^2)$. Computational time is further reduced by almost two orders of magnitude through the use of Simultaneous Perturbation Stochastic Approximation (SPSA) gradient estimation and cost-function caching. We also introduce a novel machine-learning model, and benchmark both quantum and classical approaches against a Monte Carlo baseline. The VQA outperforms the classical machine-learning approach, and performs similarly to Monte Carlo for the small networks simulated. Additionally, the results indicate a trend toward improved performance with problem size, outlining a pathway to solving larger TSP instances on quantum devices.

1 Introduction

The well-known Travelling Salesman Problem (TSP) is an important NP-Hard combinatorial optimisation problem, with industrial use cases including last-mile delivery [1] and warehousing [2]. In TSP, a salesman must visit each network location, and return to the start location, whilst minimising the cycle length. There are powerful classical solvers [3], and classical algorithms as diverse as clustering routing [4] and discrete artificial bee colony algorithm with fixed neighbourhood search [5]. Recent classical implementations have solved networks with up to 25 million locations [6]. TSP has been studied on quantum annealing devices [7–10], and with the quantum circuit-model paradigm using the hybrid Quantum Approximate Optimisation Algorithm (QAOA) algorithm [11–15]. Both quantum annealing and QAOA often use a Quadratic Unconstrained Binary Optimisation (QUBO) formulation [16]. Recent formulations use fewer qubits than QUBOs [17–22], culminating in penalty-free formulations [23–25]. Despite this work, descriptions of quantum solutions of TSP networks of more than a dozen locations in the literature are rare, and we only found two studies of circuit model simulations of networks with eight locations, neither of which achieved more than 99.7% solution quality [25, 26].

QUBO and Higher-order Unconstrained Binary Optimization (HUBO) formulations consider, and then penalise, many invalid solutions, leading to a cost function that can be difficult to optimise. Also, the often used parameter-shift optimiser can be slow, since a gradient evaluation is needed for each parameter, and this can take many shots.

This work studies simulations of a penalty-free, hybrid circuit-model Variational Quantum Algorithm (VQA), with a qubit count scaling as $\mathcal{O}(n \log_2(n))$, rather than the QUBO scaling of $\mathcal{O}(n^2)$, where there are n locations in the network. Because of the favourable scaling, only 29 qubits are required to solve a network of twelve locations, whereas the QUBO formulation would require over 100 qubits to solve a network this size.

Since shallow circuits are used, the VQA model is likely to be less prone to barren plateaus because there are fewer parameters, and more resistant to noise because of the reduced qubit count and the shallower circuits employed. We reduce computational time from over nine minutes to seven seconds for eight-location networks by deploying Simultaneous Perturbation Stochastic Approximation (SPSA) gradient estimation rather than parameter shift, and by caching cost function evaluations. The key contributions of this work are:

1. We simulate a penalty-free Variational Quantum Algorithm (VQA) using Qiskit, achieving optimal or near-optimal solutions for TSP networks of up to twelve locations in noise-free simulations. To our knowledge, this is the first successful VQA simulation of a twelve-location TSP network on circuit-model devices. The approach is also tested on noisy qubits for networks of up to nine locations, demonstrating its robustness under realistic conditions. For networks of up to nine locations we achieve 100% perfect solution quality, comparing favourable with all other circuit model studies we have found.
2. We explore different problem formulations for converting output bit strings into valid TSP cycles and distances. This includes ablation studies of factorial and non-factorial encodings, and the use of Gray encoding, providing a systematic assessment of encoding strategies for quantum TSP solutions. We achieve runtime reductions of at least 50% through caching of classical cost function evaluations.
3. Inspired by the VQA, we develop a novel classical machine-learning model capable of solving larger TSP networks than those accessible with current quantum simulations, offering a complementary approach for scalability studies.
4. We investigate VQA cost function optimisation techniques, including averaging over a subset of the lowest-cost bit strings, theoretical analysis of cost function differentiability, and comparative evaluation

of gradient estimation methods. Notably, Simultaneous Perturbation Stochastic Approximation (SPSA) reduces computational time by a factor of at least 15 over parameter-shift methods. A warm-start strategy based on classical estimates does not enhance convergence.

5. Finally, we introduce a classical Monte Carlo benchmark that samples the same number of bit strings as the VQA and ML models. This benchmark establishes a fair baseline for evaluating the performance of quantum and classical optimisation strategies, and can be applied to other quantum machine learning and optimization algorithms.

VQA simulations on Qiskit perform similarly to the Monte Carlo benchmark for up to 12 locations. Additionally, we argue that VQA is likely to outperform Monte Carlo when quantum hardware is used to implement larger networks. Calculations show that networks of up to 25 locations can be embedded on 100-qubit quantum devices.

The remainder of this document is organised as follows. Section 2, describes how the TSP is solved using quantum annealing, the quantum circuit model and bosonic sampling devices, and presents an evaluation of the limitations of existing methods. Section 3 describes our Methods, including the VQA model (Section 3.1), problem formulations (Section 3.2), the classical ML model (Section 3.3), optimisation of the cost function (Section 3.4) and estimated computational time (Section 3.5). Section 4 presents the results. Section 5 concludes the paper and discusses future work. Parameter settings are placed in Appendix A and detailed results and figures in Appendix B.

2 Solving the Travelling Salesman problem with a quantum device

The aim of the Travelling Salesman Problem (TSP) is to find the shortest Hamiltonian cycle that visits each of the n network nodes once. The network can be represented as a graph $G = (V, E)$, with each node represented as one of the V vertices in the graph, and the connections between the nodes represented as E edges. Each edge $uv \in E$ between the vertices $\{u, v\} \in V$ has a distance $D_{u,v}$. The problem is equivalent to finding a permutation π of the n nodes that minimises the distance, or cost, $C(\pi)$ shown in Equation 1, noting that $\pi(n) = \pi(0)$ because the starting location, referenced as 0, is

revisited at the end of the cycle. In this work, both vertices and nodes are described as locations.

$$C(\pi) = \sum_{i=0}^{n-1} D_{\pi(i), \pi(i+1)} \quad (1)$$

2.1 Quadratic Unconstrained Binary Optimisation

Lucas [16] formulates TSP as a Quadratic Unconstrained Binary Optimisation (QUBO) scaling as $\mathcal{O}(n^2)$. In a QUBO, the problem Hamiltonian H_P to be minimised is written as a function of binary variables x_i of no higher than quadratic order, as shown in Equation 2:

$$H_P = \sum_{i,j} Q_{i,j} x_i x_j \quad (2)$$

The problem Hamiltonian is the sum of the objective function to be minimised, and a penalty Hamiltonian to represent constraints, multiplied by arbitrary Lagrangian multipliers to ensure that it is not energetically favourable to break the constraints.

The quadratic problem formulation in Equation 2 can be mapped to an adiabatic quantum annealing device. Networks of up to a dozen locations have been solved with the D-Wave quantum annealer [7–9], and networks of up to 48 locations where some computation is offloaded to classical devices [9, 10].

In the QAOA hybrid [11–15], the time evolution of the adiabatic Hamiltonian is Trotterised using a parametrised quantum circuit with alternating layers, and the parameters are optimised classically. The problem Hamiltonian is normally the same QUBO formulation. QAOA is an example of a Variational Quantum Algorithm (VQA) [27] where parameters are optimised classically in a feedback loop. In the circuit model paradigm, the parameters are rotations [28, 29], whereas boson samplers parameterise beam splitter and/or phase shift angles [23, 30].

2.2 Non-QUBO formulations

The QUBO formulation above uses a One-Hot encoding scheme, which is inefficient since only a few binary output strings are valid solutions. Recent

proposed formulations use binary variables more efficiently, potentially allowing devices to solve larger problems [17, 18]. Higher-order Unconstrained Binary Optimization (HUBO) formulations [19–22] have reduced the number of qubits required $\mathcal{O}(n \log_2 n)$, but at the expense of more two-qubit gates.

2.3 Penalty-free formulations

In the last two years, quantum penalty-free formulations on VQAs have been implemented [23–25], with the number of qubits required scaling as $\mathcal{O}(n \log_2 n)$ where n is the number of locations, and, by design, all bit strings are mapped to valid cycles. [23] introduces a *non-factorial* penalty-free formulations as described in Section 3.2.1 and simulates this formulation for networks of up to 48 locations on a quantum boson sampler.

In contrast, [24] and [25] implement a *factorial formulation* built on earlier work [31], where the possible $n!$ permutations of the n locations are enumerated, with each permutation representing a valid cycle, as described in Section 3.2.2. The factorial formulation is simulated in [24] on a network of six locations using a Variational Quantum Eigensolver algorithm (VQE) and in [25] on a network of eight locations using Indirect Quantum Approximate Optimization Algorithm (IQAOA), a variant of QAOA. Neither simulation achieved 100% solution quality.

2.4 Other quantum approaches

Recent studies highlight the range of possible quantum algorithms available. [26] generate the uniform superposition state of all n -length Hamiltonian and claim to use very few qubits, achieving an accuracy of 99.7% for eight locations. [32] uses a Quantum-inspired Ant Colony Optimization (Qi-ACO) to solve a four-dimensional travelling salesman problem, and [33] includes quantum rotation gates and qubits into a traditional ant colony optimisation, finding that efficiency and convergence speed were enhanced. [34] uses a quantum self-attentive neural network integrated with a variational quantum circuit, trained using deep reinforcement learning algorithms, and reports reduced training parameters and dataset size while achieving superior optimisation results compared to classical methods.

2.5 Solving TSP with classical neural networks

There is a long history of solving TSP on classical neural networks. Although Hopfield networks were originally proposed in 1982 for associative memory [35], in 1985 Hopfield and Tank [36] used a Hopfield network instantiated on an analogue electrical circuit to solve TSP on what was effectively a QUBO formulation and reported simulations of network solutions of up to ten locations on an early digital computer. In 2000 [37] built on this work to find valid solutions to a 51-location TSP, on average only 15% longer than the optimal cycle. In 2008 [38] used a recurrent neural network with a *winner take all* algorithm to solve networks of up to 532 locations. In 2012 [39] found that in networks of up to 80 locations Integer Programming and Kohonen Neural Networks resulted in close to optimal solutions, whereas the Hopfield Neural Networks performed less well.

2.6 Warm starts for quantum algorithms

Barren plateaus [40] are a significant issue for VQAs. Cerezo et al. [41] argue that when a problem exhibits a barren plateau, its loss function becomes "on average, exponentially concentrated with the system size" making optimisation difficult, and that, if structures exist that avoid barren plateaus, the quantum device can be simulated classically. Rather than using a *cold start*, such as $|0\rangle^{\otimes n}$ or $|+\rangle^{\otimes n}$, a *warm start*, where an initial state $|\psi_{\text{init}}\rangle$ is derived from an approximate classical solution, may help avoid vanishing gradients with barren plateaus, as investigated in [42–45].

3 Methods

This section describes the two Variational Algorithms implemented (Section 3.1): the Variational Quantum Algorithm (VQA) (Section 3.1.1), and the classical ML model (Section 3.3). Two penalty-free formulations that map from bit strings to valid cycles are contrasted: the factorial formulation (Section 3.2.2), and the non-factorial problem formulations (Section 3.2.1). Gray encoding (Section 3.2.3) and caching (Section 3.2.4) are discussed. In the optimisation section (Section 3.4) average by slicing (Section 3.4.1) is explained, and the differentiability of the cost function is demonstrated (Section 3.4.2). Two alternative gradient descent methods for quantum: parameter shift 3.4.3 and SPSA (Section 3.4.4) are compared (Section 3.4). A warm start protocol

is described (Section 3.4.6). The computational time on quantum hardware is estimated (Section 3.5).

3.1 Variational Algorithms

A Variational Algorithm, as shown in Figure 1, is studied. A device, either quantum or classical, produces samples of bit strings, with a probability distribution dependent on the values of adjustable parameters. The parameters are optimised classically in a feedback loop. In the quantum VQA model gate rotations are parametrised (Section 3.1.1), whereas in the classical ML model (Section 3.3) the parameters are model weights. The steps followed are:

1. The device parameters are initialised with constant values or by a warm start, as explained in Section 3.4.6.
2. Bit strings are sampled from the device.
3. Bit strings are mapped to valid cycles, using either the non-factorial formulation (Section 3.2.1) or the factorial formulation (Section 3.2.2). Bit strings are interpreted as either a binary string or a Gray code (Section 3.2.3).
4. The distance for each cycle is found classically, and an average distance for the bit strings sampled is calculated. The average used is either a simple average or a fraction of the best results (Section 3.4.1).
5. The lowest distance found to date is recorded and, after a set number of iterations, the loop is terminated, and the results are output.
6. A classical optimiser uses gradient descent, as described in Section 3.4, to calculate new parameter values.
7. The device parameters are updated.
8. The cycle is re-executed from Step 2.

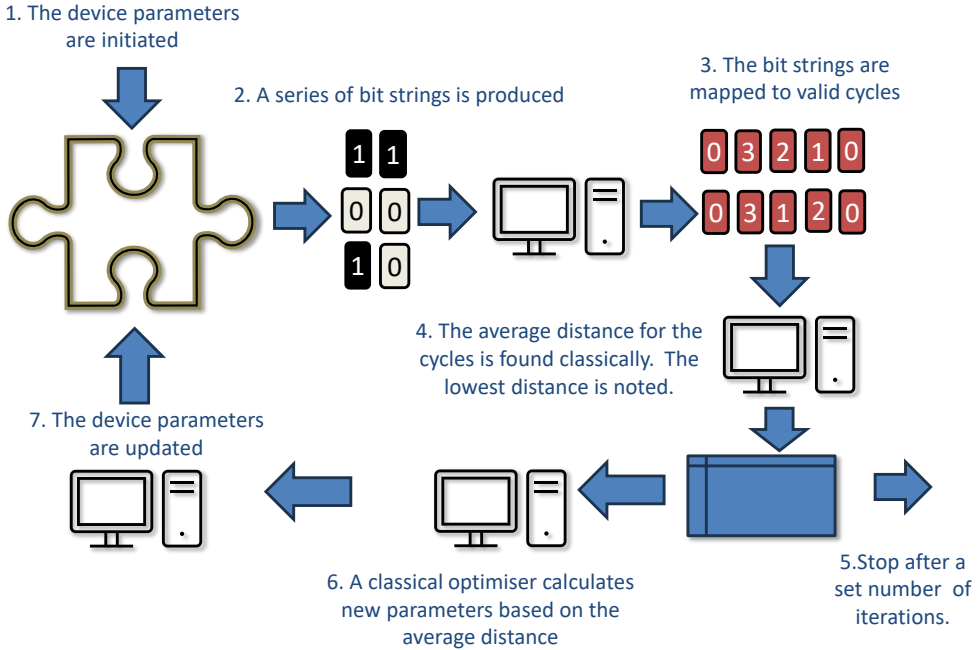


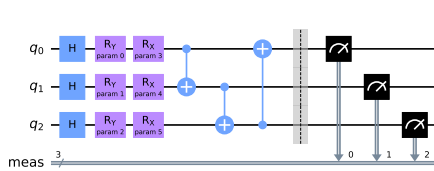
Figure 1: An overview of a Variational Algorithm, showing how either a classical or quantum device sample bit strings, which are mapped to cycles, and an average distance evaluated. A classical optimiser changes the device parameters in a feedback loop.

3.1.1 Quantum circuits in VQA

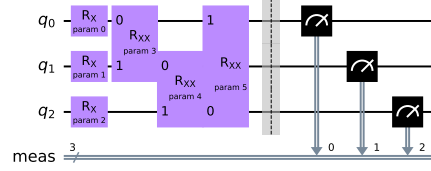
Five quantum circuits were tested in the VQA. These circuits are chosen because they are shallow, and only require limited gate connectivity: suitable for NISQ-era devices. Each RX, RY, RXX and RZZ gate has a rotation angle that can act as a tunable parameter. Circuits 1, 2 and 3 introduce entanglement, whereas circuits 4 and 5 are entanglement-free, allowing the impact of entanglement to be determined. Circuit 3 is from the well-studied IQP family, whereas Circuit 1 and 2 are of our own design.

- **Circuit 1** has a Hadamard gate, an RY and RX gate for each qubit, and an entangling CX gate linking sequential qubits (Figure 2a).

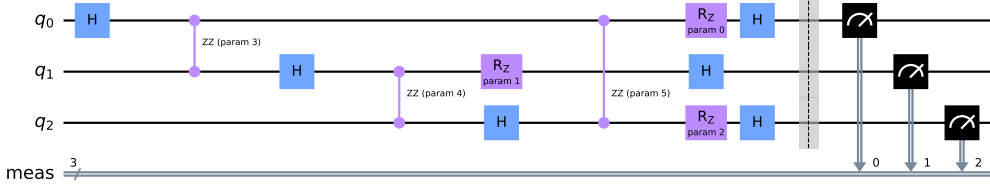
- **Circuit 2** has an RX gate for each qubit and entangling RXX gates connecting sequential qubits (Figure 2b).
- **Circuit 3** is an IQP circuit with interleaved Hadamard gates, parametrised RZ and ZZ gates (Figure 2c).
- **Circuit 4** is entanglement-free and only uses RX gates (Figure 2d).
- **Circuit 5** is also entanglement-free with H, RY and RX gates (Figure 2e).



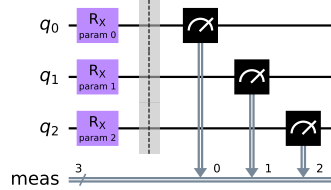
(a) **Circuit 1:** RY, RX and entangling CX



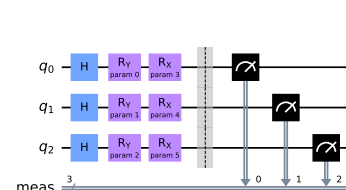
(b) **Circuit 2:** RX and entangling RXX



(c) **Circuit 3:** IQP



(d) **Circuit 4:** RX and no entangling gates



(e) **Circuit 5:** H, RY, RX and no entangling gates

3.2 Problem formulation

This section describes how a bit string is converted into a valid route, for which the distance can be evaluated. Both a non-factorial and factorial formulation are described, as well as Gray encoding. Computation time is reduced by caching classical distance evaluations.

3.2.1 Non-Factorial Formulations without penalty terms

A non-factorial formulation without penalty terms is implemented, following [23]. Location references are moved from an initial sequential list to a reordered list until the initial list is empty and the reordered list contains a valid cycle, as described in Algorithm 0 and shown in Figure 3. This is done by splitting the bit string sampled from the quantum device into smaller strings, which are interpreted as the binary encoding of indices that point to the next item of the ordered list to be moved. The use of modulo arithmetic prevents errors where the index is too high to reference a valid element of the ordered list. The bit string length l_b required is calculated as shown in Equation 3:

$$l_b = \sum_{i=1}^{n-1} \lceil \log_2(i) \rceil \quad (3)$$

Algorithm 0: Non-factorial formulation from [23]. This algorithm receives a bit string b of length l_b as defined in Equation 3, and the number of locations n as an input. The output is a permutation of the numbers $\{0, \dots, n - 1\}$, which can be interpreted as a cycle in a TSP with n locations. This algorithm uses zero-based indexing

Data: Bit string b of length l_b , number of locations n

Result: TSP Cycle s

$cycle \leftarrow (1, \dots, n - 1)$, $s \leftarrow (0)$, $i \leftarrow n - 1$;

while $i > 1$ **do**

$b_{temp} \leftarrow ()$;
Append $\lceil \log_2(i) \rceil$ bits from b to b_{temp} ;
Delete $\lceil \log_2(i) \rceil$ bits from b ;
Evaluate b_{temp} as an integer j ;
 $k \leftarrow j \bmod(i)$;

Append $cycle_k$ to s ;

Delete $cycle_k$;

$i \leftarrow i - 1$;

Append $cycle_0$ to s ;

The non-factorial formulation

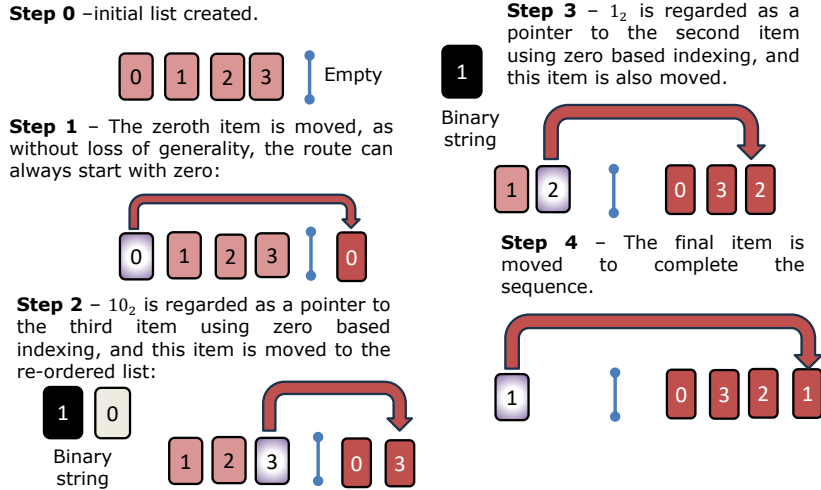


Figure 3: **Algorithm 1:** Diagram showing how the bit string 10_21_2 is used to construct a cycle by using the bit string to point to the next item of the ordered list to be moved

3.2.2 The factorial formulation

In contrast to the *non-factorial formulation*, [24] and [25] use a *factorial formulation* to enumerate the possible $n!$ permutations of the n locations, noting that each permutation represents a valid cycle. By generalising standard positional number systems, such as decimal, an index x that identifies a unique permutation can be written as shown in Equation 4:

$$x = \sum_{i=1}^{i=n} a_i i! \quad (4)$$

where $a_i \leq i!$. Algorithm 1 shows how the a_i are calculated for a binary string generated by a quantum device, and are used to identify items to be moved from an initial sequential list to a re-ordered list.

Algorithm 1: Factorial formulation based on Schnaus et al. [24].

This algorithm receives a measured state x , which is interpreted as a binary number, and the total number of locations n as an input. The output is a permutation of the numbers $\{1, \dots, n\}$, which can be interpreted as a cycle in a TSP with n nodes. The formulation in the original paper has been slightly modified.

Data: Index x , number of locations n

Result: TSP Cycle s

```
 $f \leftarrow n!$ ,  $y \leftarrow x \bmod f$ ;  
 $nodes \leftarrow (1, \dots, n)$ ,  $s \leftarrow ()$ ,  $i \leftarrow 0$ ;  
while  $i < n$  do  
   $f \leftarrow \frac{f}{n-i}$ ;  
   $k \leftarrow \lfloor \frac{y}{f} \rfloor$ ;  
  Append  $cycle_k$  to  $s$ ;  
  Delete  $cycle_k$ ;  
   $y \leftarrow y - kf$ ;  
   $i \leftarrow i + 1$ ;
```

3.2.3 Gray encoding

To interpret bit strings as a numerical index two approaches are compared: a standard binary coding, where the bit string is regarded as the binary representation of a number; and Gray encoding, a bijective map between bit strings to numbers, designed so that as the number is increased by one, only one bit of the string changes.

3.2.4 Caching

The classical mapping of a bit string to a cycle, and the calculation of the distance for that cycle may be performed many times for a particular bit string. To reduce computational time, the results for each bit string are cached in memory. A custom implementation is required because the Last Recently Used (LRU) cache provided by the `@lru_cache` decorator in the Python `functools` package assumes that the key of the cache table is a string, whereas in our code, the key is a list output by Qiskit.

3.3 Classical machine model

A novel classical machine language (ML) model inspired by VQA is shown in Figure 4. The ML model has the same number of inputs and outputs as the VQA model and uses fully connected layers, a sine activation function inspired by the quantum model, and produces a binary output by comparing the output of each activation layer to a random number.

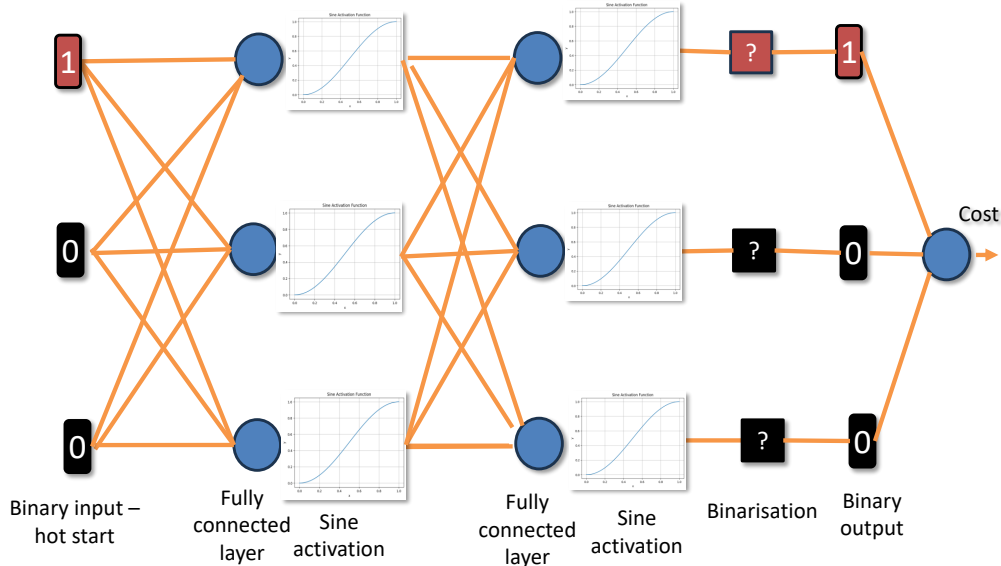


Figure 4: A classical machine learning circuit with two fully connected layers, Sine activation, binarisation, and objective function evaluation

3.3.1 Input and fully connected layer

The input data are structured as a $N_s \times q$ PyTorch tensor, comprising N_s identical vectors of dimension q , where q is the number of binary variables required to model the n locations. The number of input vectors N_s is equivalent to the number of shots in the quantum model, or an ML mini-batch, and

is a tunable hyper-parameter. The number of binary variables, q , is equivalent to the number of qubits in the quantum algorithm. The circuit is shown in Figure 4 where $q = 3$. With a warm start, each element of the input is initialised by setting all biases and weights to zero, except for the weights for the diagonal elements of the adjacency matrix for the fully connected layer, which are set to 1, so that the input bit strings propagate to the output of the model. If there is no warm start the input is either set to 0, or to 0.5 and PyTorch automatically initialises the weights and biases. The input is fed into a fully connected layer with q inputs and q outputs.

3.3.2 Activation function

To introduce non-linearity, a Sine activation function mimics the trigonometric rotations of quantum devices.

3.3.3 Binarisation

The output of the model is binarised depends on whether the input x is greater than a random number u from a uniform distribution in the interval $[0, 1)$ as shown in Equation 5:

$$g(x) = \begin{cases} 1, & \text{if } x > u \\ 0, & \text{otherwise} \end{cases} \quad (5)$$

The model is coded in PyTorch [46] and the gradients for the fully connected layer and the Sine activation are calculated automatically as standard. The correct value for the gradient of binarisation is $g(x) = x + (g(x) - x)$ and so $g(x) - x$ is detached from the computational graph, used to compute gradients, ensuring the gradient is correctly evaluated as the gradient of x .

3.3.4 Distance evaluation

Similarly to the input vector, the data after binarisation is structured as a $N_s \times q$ tensor comprising N_s output binary vectors of dimension q . Let \mathbf{x}_i denote the i^{th} binary output vector where $\mathbf{x}_i \in \{0, 1\}^q$. $x_i^{(j)}$ refers to the j^{th} bit of \mathbf{x}_i . Each of the N_s binary output vectors is mapped to a valid cycle and the distance for that cycle is evaluated using a classical function module represented as a function $h : \{0, 1\}^q \mapsto \mathbb{R}$. The final output of the model at

the end of each iteration is a simple average \bar{d} of the distances calculated, as shown in Equation 7, and described in Section 3.4.1 below.

Bespoke coding is needed to calculate and save the gradient in the forward pass and to retrieve the saved tensor in the backward pass. The j^{th} component of the i^{th} gradient vector is calculated by flipping the j^{th} bit and evaluating the cost function before and after the bit-flip as shown in Equation 6, where \oplus represents a bitwise XOR, and $\mathbf{e}^{(j)}$ represents the standard basis vector with 1 in the j^{th} position and 0 elsewhere, noting that $2x_i^{(j)} - 1 : \{0, 1\} \mapsto \{-1, 1\}$ is an adjustment that ensures the sign is correct.

$$\frac{\partial h}{\partial x_i^{(j)}} = \frac{h(\mathbf{x}_i) - h(\mathbf{x}_i \oplus \mathbf{e}^{(j)})}{2x_i^{(j)} - 1} \quad (6)$$

3.3.5 Computational graph

The completed computation graph for a model with one layers produced using Torchviz [47] with $N_s = 1,024$ and $q = 3$ is shown in Figure 8 in Appendix C.

3.3.6 Gradient descent for ML

The standard PyTorch optimiser for gradient descent with SGD and Adam are compared. In addition to the learning rate, the momentum and weight decay, an L2 penalty against weights, are treated as hyper-parameters. SPSA was not investigated because SPSA would not have allowed back-propagation, an intrinsic part of the ML algorithm.

3.4 Optimisation

3.4.1 Averaging by slicing

Each shot (bit string sampled) in an iteration could have a different cycle and a different distance. The default average \bar{d} over the N_s shots in an iteration is shown in Equation 7, recalling that $h : \{0, 1\}^n \mapsto \mathbb{R}$ is the function that assigns a scalar output to each bit string \mathbf{x}_i by mapping the bit string to a valid cycle, and finding the distance for that cycle.

$$\bar{d} = \frac{1}{N_s} \sum_{i=1}^{N_s} h(\mathbf{x}_i) \quad (7)$$

Alternatively, the outputs $\{h(\mathbf{x}_i)\}$ can be listed in ascending order of distance $[d_k]$ with only a fraction, or *slice*, of the results used in the average, possibly reducing the sample noise. The average \bar{d}_S is calculated as shown in Equation 8 where N is the number of shots and S is the slice fraction with $0 \leq S \leq 1$.

$$\bar{d}_S = \frac{1}{SN_s} \sum_{k=1}^{SN_s} d_k \quad (8)$$

For example, if $S = 1$ the optimiser uses the simple average over all shots, if $S = 0.8$ the optimiser uses the average over the 80% of the shots with the lowest distance. Both the simple average and average by slicing are assessed.

3.4.2 Differentiability of the cost function

It is known that in hybrid algorithms such as Quantum Variational Eigen-solver (QVE) and QAOA, the weighted sum of the measured expectation values can be minimised by tuning the parameters $\boldsymbol{\theta}$ [48]. However, with VQE and QAOA, the quantity being optimised is a quantum observable, whereas the VQA model studied optimises an output, written as $\mathcal{H}(\boldsymbol{\theta})$, obtained by mapping each bit string sampled to a valid cycle, and averaging the calculated distance over many samples to yield an estimate of the expected value, as defined in Equations 7 and 8. It is therefore necessary to demonstrate that the output of the VQA model is differentiable.

Our quantum circuits effect a unitary transformation $U(\boldsymbol{\theta})$ on an input $|\psi_{\text{in}}\rangle$. Repeated measurement of the output wave function produce a series of classical bit strings $\mathbf{x}_i \in \{0, 1\}^n$, each corresponding to an output wave function $|x_i\rangle$ with probability $p_i(\boldsymbol{\theta})$, given by Born's rule in Equation 9, where $p(\boldsymbol{\theta})$ denotes the probability distribution from sampling the output bit strings:

$$p_i(\boldsymbol{\theta}) = |\langle x_i | U(\boldsymbol{\theta}) | \psi_{\text{in}} \rangle|^2 \quad (9)$$

The expected output is defined by rearranging Equation 7 as Equation 10:

$$\hat{\mathcal{H}}(\boldsymbol{\theta}) := \bar{d} = \mathbb{E}_{\mathbf{x}_i \sim p(\boldsymbol{\theta})} \sum_{\mathbf{x}_i} p_i(\boldsymbol{\theta}) \cdot h(\mathbf{x}_i). \quad (10)$$

The function $\theta \mapsto p_i(\theta)$ is differentiable, since the VQA model uses parametrised quantum circuits with smooth gates [48]. $h(\mathbf{x}_i)$ does not depend on θ , so the expected output θ is also differentiable and its gradient is:

$$\frac{d\hat{\mathcal{H}}(\theta)}{d\theta} = \mathbb{E}_{\mathbf{x}_i \sim p(\theta)} \sum_{\mathbf{x}_i} \frac{dp_i(\theta)}{d\theta} \cdot h(\mathbf{x}_i). \quad (11)$$

The expectation value estimated in Equation 10, uses sampling using a finite number of shots (N_S) over a probability distribution $p(\theta)$. Although this estimator is not strictly differentiable since it is based on finite samples, experience from quantum machine learning has shown that unbiased estimators of the gradient can be computed using methods such as the parameter-shift rule. This generalisation might not apply to slicing (Equation 8), since only a subset of the sample is considered.

This establishes that for the VQA model studied, the expected value of the output of the quantum device $\hat{\mathcal{H}}(\theta)$ can be treated as differentiable. Now we know it is meaningful to discuss a gradient, we compare two gradient estimation methods: parameter shift and SPSA.

3.4.3 Parameter Shift gradient estimation

A standard method for evaluating the gradient of quantum circuits is the parameter shift rule [49]. The i^{th} component of the gradient $\nabla_t(\theta_t)$ for the cost function $\mathcal{H}(\theta)$ in the t^{th} iteration is shown in Equation 12, where \mathbf{e}_i is a standard basis vector with all zeros except one at the i^{th} position, s is a hyper-parameter with a default value of 0.5 and $\langle \dots \rangle$ denotes an expectation value estimated by averaging over a number of shots. **Bold** is used to denote vectors such as ∇_t , θ_t and \mathbf{e}_i .

$$[\nabla_t(\theta_t)]_i = s \left[\langle \mathcal{H} \left(\theta_t + \mathbf{e}_i \frac{\pi}{4s} \right) \rangle - \langle \mathcal{H} \left(\theta_t - \mathbf{e}_i \frac{\pi}{4s} \right) \rangle \right] \quad (12)$$

The iterative update to the parameter vector θ_t at the t^{th} iteration is given by equation 13 where η is the learning rate, a hyper-parameter.

$$\theta_{t+1} = \theta_t - \eta \nabla_t(\theta_t) \quad (13)$$

3.4.4 Simultaneous Perturbation Stochastic Approximation gradient estimation

Parameter shift is a computationally expensive method for evaluating gradients because, for each parameter, two valuations of the cost function are required, and each valuation requires multiple shots of the quantum device. By contrast, the Simultaneous Perturbation Stochastic Approximation (SPSA) technique requires only two valuations of the cost function for each iteration, independent of the number of parameters.

In SPSA [50] the iterative update to the parameter vector $\boldsymbol{\theta}_t$ is given by equation 14 where $\nabla_t(\boldsymbol{\theta}_t)$ is an estimate of the gradient in the t^{th} iteration.

$$\boldsymbol{\theta}_{t+1} = \boldsymbol{\theta}_t - a_t \nabla_t(\boldsymbol{\theta}_t) \quad (14)$$

The i^{th} component of the gradient in the t^{th} iteration is given in Equation 15 where \mathcal{H} is the cost function and Δ_t is a random perturbation vector with $[\Delta_t]_i \in \{-1, 1\}$. Only two cost estimates are required.

$$[\nabla_t(\boldsymbol{\theta}_t)]_i = \frac{\langle \mathcal{H}(\boldsymbol{\theta}_t + c_t \Delta_t) \rangle - \langle \mathcal{H}(\boldsymbol{\theta}_t - c_t \Delta_t) \rangle}{2c_t [\Delta_t]_i} \quad (15)$$

Both $\{a_t\}$ and $\{c_t\}$ are positive number sequences converging to zero, ensuring that both the learning rate and the gradient inputs reduce with iteration, and are defined in equations 16 and 18 respectively. A , c , α , η , and γ are hyper-parameters and G_0 denotes the mean absolute value of the components of the initial gradient. In rare cases G_0 , as defined in equation 17 can be evaluated at zero and is then redefined as a large arbitrarily high value to avoid division by zero.

$$a_t = \frac{a}{(t + 1 + A)^\alpha} \quad \text{where } a = \eta \frac{(A + 1)^\alpha}{G_0} \quad \text{with} \quad (16)$$

$$G_0 = \frac{1}{n} \sum_{i=1}^n |[\nabla_0(\boldsymbol{\theta}_0)]_i| \quad (17)$$

$$c_t = \frac{c}{(t + 1)^\gamma} \quad (18)$$

A bespoke version of SPSA was coded in Python to enable hyper-parameter tuning.

3.4.5 Hyper-parameter tuning

The hyper-parameters of the optimiser described in Sections 3.4.3, 3.4.4 and 3.3.6 were varied to find the best values. The slice described in section 3.4.1 was varied for the quantum model.

3.4.6 Warm start

A warm start may help optimisation by reducing the impact of barren plateaus (Section 2.6). To achieve a warm start, a greedy "nearest neighbour" classical algorithm finds a warm start cycle by iteratively selecting the nearest network location. The corresponding warm-start bit string is found by reversing the mapping from bit string to cycle. The distance found by this greedy algorithm is compared against the results of the simulations.

The warm start is loaded onto quantum circuit 2 by initialising the RXX gate rotations to 0, and setting the RX gate rotations to zero, if the corresponding bit is 0, and to π if the corresponding bit is 1; and onto the ML model as described in Section 3.3.1

3.5 Estimated computational time

With SPSA two gradient evaluations are performed for each of the I iterations, as well as evaluations of the sliced and average cost. With n_{shot} shots for each iteration, the total number of shots N_{shots} is given by $4In_{shot}$. If each shot takes time t_{shot} , a rough estimate of the expected algorithm completion time T is given by $4In_{shot}t_{shot}$ which does not depend on the network size. IBM documentation [51] implies $t_{shot} \approx 2\text{ }\mu\text{s}$. Other relevant parameters are $I = 250$ and $n_{shot} = 1,024$. The VQA could take seconds to run assuming close integration between classical and quantum processing.

By contrast, with parameter shift, the timing will scale less favourably with the number of locations as $\mathcal{O}(n\log_2 n)$ where n is the number of locations, because each qubit will have one or more parameters.

4 Results

4.1 Summary of results

The results of simulations of the VQA and ML model are compared with classical Monte Carlo and Greedy methods (Section 4.3). The VQA model finds high solutions for networks of up to twelve locations, and did not outperform Monte Carlo. Caching the classical cost evaluation and SPSA reduces computational time (Section 4.4.1). The default slicing ratio of 1 may be sub-optimal (Section 4.4.4). Little impact on solution quality is found from using either the factorial and non-factorial formulation (Section 4.4.5), warm starts (Section 4.4.6, and Gray encoding (Section 4.4.8).

4.2 Experimental setup

4.2.1 Hyper-parameters used

All simulations are, unless otherwise stated, run with the default values shown in Table 3 in Appendix A found after hyper-parameter optimisation.

4.2.2 Data

VQA is simulated with networks from four to twelve locations, and the classical ML model is run on networks up to 48 locations with datasets sourced from [23] and [52], and our own datasets manufactured by randomly sampling n locations from a 100×100 grid using a uniform probability distribution.

4.2.3 Hardware

The simulations are run on a laptop with an Intel Core(TM) i5-10210U CPU clocked at 1.60 GHz with 8.00 GB (7.76 GB usable) RAM running Windows 11 and equipped with an NVIDIA GeForce GTX 1650 GPU. NVIDIA CUDA is enabled for the PyTorch classical machine learning experiments.

4.2.4 Software

The notebooks and relevant Python modules are placed on GitHub [53]. The quantum circuits are coded in Qiskit [54] using `SamplerV2` from `qiskit_aer.primitives` for noise-free runs. For noisy runs, the circuit are transpiled onto the `FakeAuckland`

digital twin of the IBM Auckland processer to use the IBM gate set, and then `qiskit_ibm_runtime` is used with the same fake back-end to access device-specific noise levels. `FakeAuckland` was chosen because it has 27 qubits and a representative IBM topology. The classical machine learning circuits are coded in PyTorch [46].

4.2.5 Monte Carlo benchmark

The simulation results of both VQA and ML models are benchmarked by a Monte Carlo evaluation, by taking the maximum number of bit strings these models sampled for a given number of locations, and iterating over these random bit strings to find a minimum distance using the non-factorial formulation. A Python method coded in the caching class (Section 3.2.4) evaluates the number of bits strings sampled by our models. The number of bit strings sampled varies, because each shot might return from 1 to 2^q , bit strings, where q is the number of qubits.

A coverage $\mathcal{C} = \frac{H+M}{P(n)}$ is reported, where H is the number of hits to the cache, M is the number of cache misses, and $P(n) = \frac{(n-1)!}{2}$ is the total number of unique cycles through a network with n locations. If $\mathcal{C} > 1$ then more bit strings are sampled than unique cycles through the network, and instead the results for each bit string could have been enumerated and the shortest cycle identified.

4.2.6 Solution quality metric

The quality of the solution is defined as $Q_{sol} = \frac{D_{best}}{D_{sim}}$. The minimum simulation distance found (D_{sim}) is compared with the best known minimum distance (D_{best}) taken from the datasets [23] [52], or by brute force enumeration over all cycles for our own datasets. A solution quality of $Q_{sol} = 1$ represents a solution where the shortest distance found is optimal, and a value less than 1 represents a suboptimal solution. Since the quality of the solution is often close to 1, it is sometimes more helpful to consider the solution error $E_{sol} = 1 - Q_{sol}$.

4.2.7 Estimated sample error

The runs are stochastic because of the inherent probabilistic nature of quantum computing and stochastic gradient descent, where used. Where r runs

are carried out for the same set of parameters, an estimate of the sample error of the mean $SEM = \frac{\sigma}{\sqrt{r-1}}$ is provided where σ is the observed standard deviation.

4.3 Model comparison

During the hyper-parameter optimisation Circuit 2 was chosen as the best performing circuit and so was selected for study. In fact, it was later found, when more runs were executed, that the five quantum circuits studied have broadly comparable solution qualities (Section B.1). A comparison of the solution quality for both noisy and noise-less simulations of Qiskit with Circuit 2, the Monte Carlo benchmark (Section 4.2.5) with comparable bit strings and the Greedy Classical algorithm is shown in Table 1a. We find 100% solution quality for our simulations for up to nine locations. As discussed in Section 2 we did not find other studies that simulated more than eight locations, and these reported sub-optimal solutions [25, 26]. The solution quality for the classical machine learning model (ML), compared to the Monte Carlo benchmark, and Greedy classical algorithm is shown in Table 1b.

Locations	Noise free qubits	Noisy qubits	Monte Carlo	Greedy
4 to 9	100.0 ± 0.0	100.0	100.0 ± 0.0	< 100
10	99.5 ± 0.4	n/a	99.6 ± 0.5	92.9
11	99.5 ± 0.3	n/a	98.7 ± 0.2	84.6
12	93.5 ± 0.8	n/a	94.0 ± 0.1	77.1

(a) Average solution quality for VQA networks with noise-free and noisy Qiskit simulations of the quantum circuit 2

Locations	Classical ML	Monte Carlo	Greedy
4 to 9	100.0 ± 0.0	100.0 ± 0.0	< 100
10	97.5 ± 1.1	100.0 ± 0.0	92.9
11	98.7 ± 0.2	100.0 ± 0.0	84.6
12	90.7 ± 1.8	98.9 ± 0.5	77.1
15	74.7 ± 1.7	81.6 ± 0.5	100.0
17	82.7 ± 6.1	87.9 ± 1.0	95.3
26	90.6 ± 1.8	62.8 ± 1.3	84.3
42	100.0 ± 0.0	38.2 ± 0.6	73.1
48	10.3 ± 0.2	11.2 ± 0.25	26.2

(b) Average solution quality for Classical ML model with 1,024 shots

Table 1: Comparison between the average solution quality for networks with different number of locations with the classical ML model and VQA, Monte Carlo baseline using a comparable number of total bit strings sampled and a greedy classical model.

Figure 5 plotted from Tables 1a and 1b compares the results of simulations of the VQA model, the classical ML model, the Monte Carlo benchmark, and a greedy nearest neighbour algorithm (Section 3.4.6). In the Monte Carlo benchmark of the ML model the benchmarks are higher than for the quantum benchmarks because the ML model samples more bit string than VQA. The Monte Carlo and greedy algorithms are far from the best classical algorithms, and outperforming them is a necessary, but not sufficient condition, for an eventual quantum advantage.

With noise-free qubits (Section B.1 in Appendix B) the VQA model found

high solutions for networks up to twelve locations, only limited by the number of qubits it was possible to simulate in Qiskit, and the best quantum circuit always outperforms a greedy classical algorithm.

With noisy simulations using the `FakeAuckland` IBM fake backend, only nine locations could be simulated because larger circuits took too long to run. Perfect solutions were found for these simulations, albeit more bit strings were sampled than the total solution space, as described above. On larger networks run with a more powerful simulator noisy and noise free solution qualities seem likely to be similar, based on the simulation of the smaller networks.

Perfect results were found for the ML model for the network with 42 locations. By plotting the relevant data set `dantzig42_xy.csv` it was found that ordering the locations in numerical order gave close to the optimum solution and this is an easy solution to find for our formulation.

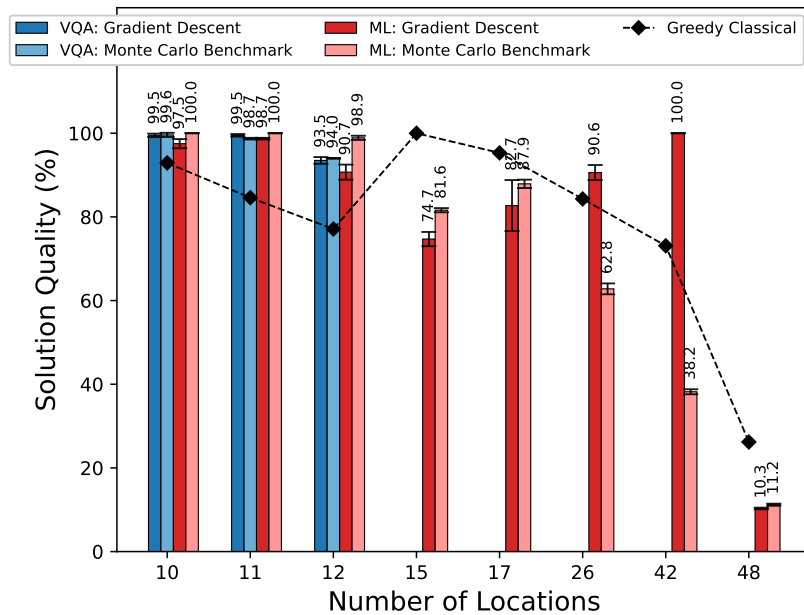


Figure 5: Solution quality by locations comparing our VQA and ML models with their Monte Carlo benchmarks, and a Greedy classical.

4.3.1 VQA performance against Monte Carlo for larger networks

There are no significant differences between the solution quality of our VQA model using gradient descent and the equivalent Monte Carlo benchmark for up to twelve locations. Figure 6 plotted from the data in Table 17 in Appendix B shows that the total number of bit strings sampled with the VQA model with SPSA is bounded by $4In_{shot}$ (section 3.5), while the total size of the solution space grows very quickly. We predict that the quality of the solution of the VQA Monte Carlo benchmark will decline much faster than our gradient descent VQA model because Monte Carlo samples a rapidly decreasing fraction of the solution space. In contrast, our models benefit from gradient descent to purposefully search the cost function for the optimum value. Figure 5 shows that this happens with our gradient descent classical ML model. It can be seen from Figure 7 that the gradient descent in VQA is effective: the average distance found reduces as the simulation progresses.

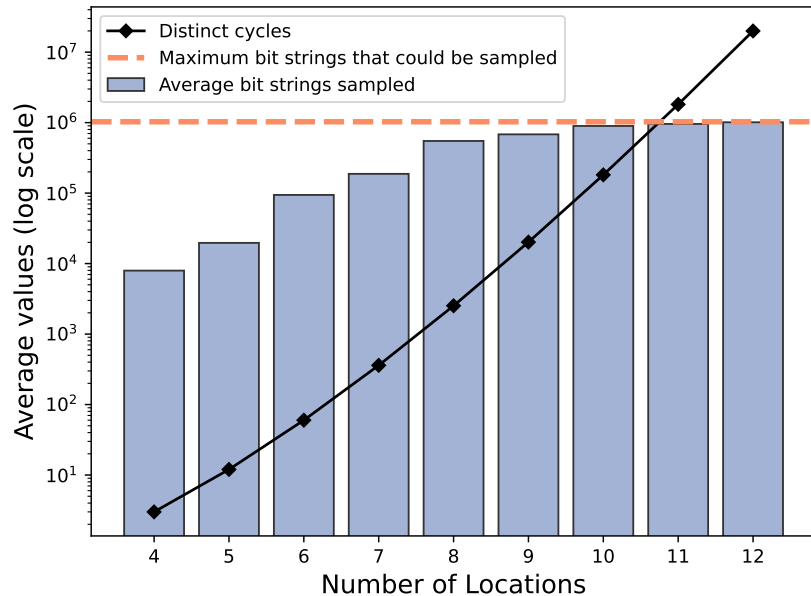


Figure 6: Binary strings sampled by the VQA model and distinct cycles by location. As the size of the networks increases the number of binary strings required by VQA approaches an upper limit, whereas the number of distinct cycles grows rapidly.

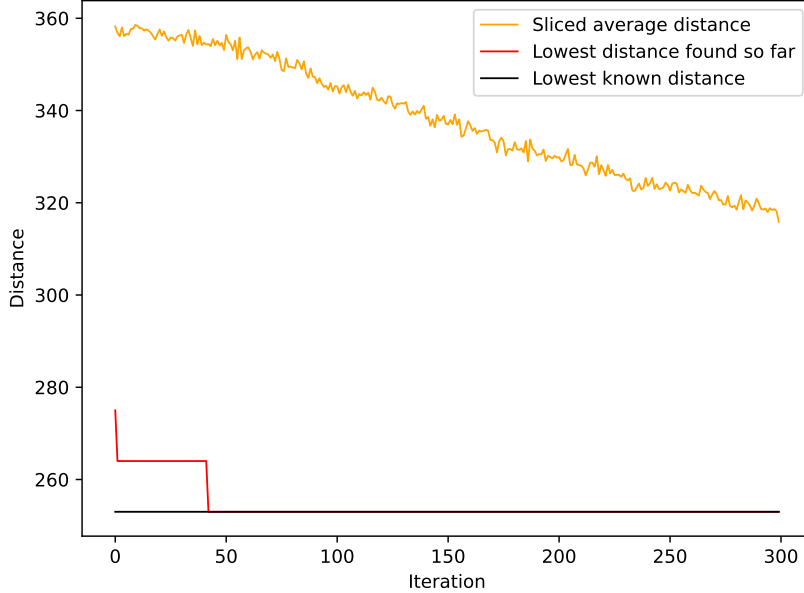


Figure 7: Plot of sliced average distance and lowest distances for the VQA model in a network with eleven locations and default parameters showing that the gradient descent is effective

4.4 Ablation Studies and Optimisation Performance

This section describes the results of ablation studies that systematically vary key model components to assess their impact.

4.4.1 Computational time decreases

The use of caching and SPSA significantly reduced overall run times from more than 9 minutes to seven seconds, as shown in Table 2. The table shows the timings for four runs with eight locations with SPSA and Parameter Shift gradient descent, as described in Section 3.4. Caching the classical cost evaluation of the distance for bit string significantly reduces run-time, for example from 37 seconds to 7 seconds with SPSA and was used by default.

	SPSA	Parameter shift
No caching	37 secs	585 secs
Caching	7 secs	217 secs

Table 2: Table for a network with eight locations showing caching significantly reduces run times, for different gradient descent methods. SPSA is quicker than parameter shift.

4.4.2 Hyper-parameter tuning results for VQAs

For the parameter-shift optimiser the learning rate η was varied whilst keeping s constant. Then s was varied using the best value found for η . The standard choice of 0.5 appeared to work well. For the SPSA optimiser, A and η were varied in a logarithmic grid search. Once the best values for these were found, α , γ and c were also varied. The optimum hyper-parameters found are given in Table 3 in Appendix B. High quality solutions were found with standard values of α, γ and c .

The parameter shift optimiser was found to take a long time to run, as expected (see Table 2) because multiple shots of the quantum device were needed, one for each parameter. Moreover, it was often noted that the cost function did not converge to a set value. Because SPSA gave high quality solutions and was much faster, SPSA was used as the default parameter.

4.4.3 Hyper-parameter tuning results for ML

For classical machine learning, SGD and Adam are investigated, as described by Goodfellow et al. in the context of deep learning [55]. For SGD, the changes in momenta β , the learning rate η , and the weight decay λ were investigated. For Adam a standard momentum β_1 of 0.9 was used and a logarithmic grid search was performed for the learning rate η and the weight decay λ . In both cases it was important to use a non-zero weight decay, this may be because it is important to keep the weights small for stability in training, because the *Sine* activation layer maps multiple of 2π to the same value. The best value for σ , the variability of the initial variables in the warm start for the ML model was found to be 0.05.

4.4.4 Slicing

Figure 9 in Appendix C shows the average error by location for different slices as defined in Section 3.4.1. For networks with twelve locations, where the errors are higher, it can be seen that the default slicing ratio of 1 may be sub-optimal, with slicing ratios of 0.4, 0.7, 0.8 and 0.9 giving better results. However, the results for smaller networks are inconsistent, possibly because the errors are small. At least five data runs were performed for each slice and location combination, and the error bars shown are the standard error for that combination. The number of runs was kept low because the simulations of the larger networks were computationally demanding. The average error rates are very low for networks with less than nine locations; therefore, these simulations are omitted from the plot.

4.4.5 Factorial and non-factorial formulation

The quality of the solution for networks of different sizes with VQA and ML models using both factorial and non-factorial formulations is shown in Table 6 in the Appendix B. It can be seen that there is little difference in the solution quality of the factorial and non-factorial formulations. In addition to solution quality, the number of qubits required by each formulation is important. Table 7 in Appendix B shows the qubits required for different network sizes for the factorial and non-factorial formulation. It can be seen that for small location sizes the non-factorial formulation requires fewer qubits, and this is reversed for networks with more than 15 locations. *Solving a network of 25 locations on quantum hardware may require as few as 84 qubits.*

Table 17 in Appendix B shows that the number of distinct cycles quickly becomes very large. We speculate that with the factorial formulation, carrying out arithmetic operations of numbers of this size without rounding may require significant memory and time, and become infeasible for very large networks. This means that the non-factorial formulation may be more appropriate for future large scale implementations on quantum hardware.

4.4.6 Warm start

The use of warm start slightly decreases the solution quality of the VQA model and slightly increases the solution quality of the ML model, although the differences are small, as shown in Tables 8 and 9 in Appendix B. It was found that our warm start binary string is not close to the binary string of the

optimum solution by comparing the Hamming distance: the number of positions where corresponding bits are different. Table 10 in Appendix B shows that, apart from a trivial network of four locations, the Hamming distance between the warm start binary string and the optimum binary string, found by brute-force, was at least a third of the total number of binary variables.

4.4.7 Classical ML model

Section B.3 describes how adding more layers to the classical ML model does not significantly affect the quality of the solution, and changing the number of binary vectors, or shots, in each epoch by the classical ML model improves the quality of the solution, at the cost of longer run times.

4.4.8 Gray encoding

The quality of the solution of networks of different sizes with quantum and ML models with and without Gray codes is shown in Table 11 in Appendix B. It can be seen that the use of Gray codes hardly affects the quality of the solution. The average solution quality is lower for the ML model because this model could solve larger networks, which means the averages are not directly comparable.

5 Conclusion and future work

Simulations of our VQA model on TSP networks have shown high solution qualities. Networks of up to twelve locations with noise-free qubits, and networks of up to nine locations with noisy qubits, have been simulated, limited only by the performance of Qiskit on our laptop. The VQA model has shallow circuits and relatively few qubits, reducing the dimensionality of the parameter space, helping mitigate against barren plateaus, and improving the noise-tolerance. A quantum-inspired classical ML model has also been implemented to benchmark the VQA’s performance, and although it does not outperform the VQA, it provides a useful classical baseline.

A crucial benchmark has also been established by comparing the average solution quality of our models against a Monte Carlo benchmark, which evaluates a cost by sampling a comparable number of bit strings and finds the minimum cost for every bit string sampled. Although the VQA model studied does not outperform Monte Carlo for the relatively small networks

studied (falling short by about only 0.1% at ten locations and 0.5% at twelve locations), it is expected to outperform Monte Carlo when run on quantum hardware for larger networks, establishing a roadmap to quantum TSP solutions for larger networks than currently possible.

In future work, with larger networks, it might be appropriate to investigate other optimisation schemes, since [56] found that SPSA is best with a small number of parameters, and CSM-ES and PEPG are better for more complex models. Although initialising our algorithm using "nearest neighbour" warm starts did not show an advantage, there are more sophisticated classical approaches to finding approximate solutions for TSP [57]. These could be explored in future work to assess if there are better ways to find warm starts, minimising the impact of barren plateaus [40, 41]. Future work might also investigate improving the performance of our classical machine learning model by initialising weights following Sitzmann [58] for Sine activations, rather than the Kaiming-He Uniform Initialisation [59] used as default by PyTorch for Linear layers. Markovian bit string generators can also produce correlated bit strings [60]. Markov chains could be investigated in future work to confirm that they do not outperform our model.

6 Acknowledgments

Many thanks to Manuel Schnaus for helpful input on his formulation of TSP. IBM® and Qiskit® are registered trademarks of International Business Machines Corp. NVIDIA®, GeForce® and CUDA® are registered trademarks of NVIDIA. Intel® is a registered trademark of Intel Corporation.

7 References

References

- [1] Zhiyuan Shi, Shaozhi Hong, Zeling Wang, and Ang Li. Exact solution approaches for the traveling salesman problem with a drone station. *European Journal of Operational Research*, 328(3):845–861, February 2026.
- [2] Stefan Bock, Stefan Bomsdorf, Nils Boysen, and Michael Schneider. A survey on the Traveling Salesman Problem and its variants in a ware-

housing context. *European Journal of Operational Research*, 322(1):1–14, April 2025.

- [3] Applegate D L, Bixby R E, Chvátal V, and Cook W J. Concorde TSP Solver, 1997. Available at <https://www.math.uwaterloo.ca/tsp/concorde.html>.
- [4] Prasanta Dutta, Indadul Khan, Krishnendu Basuli, and Manas Kumar Maiti. A heuristic with clustering-routing approach for the Multi-depot Multiple Traveling Salesman Problems in different fields. *Engineering Applications of Artificial Intelligence*, 160:112013, November 2025.
- [5] Xing Li, Shaoping Zhang, and Peng Shao. Discrete artificial bee colony algorithm with fixed neighborhood search for traveling salesman problem. *Engineering Applications of Artificial Intelligence*, 131:107816, May 2024.
- [6] David Applegate, William Cook, and André Rohe. Chained Lin-Kernighan for Large Traveling Salesman Problems. *INFORMS J. on Computing*, 15(1):82–92, January 2003.
- [7] Alessia Ciacco, Francesca Guerriero, and Francesco Paolo Saccomanno. Quantum annealing for the two-level facility location problem. *Future Generation Computer Systems*, 174:107961, January 2026.
- [8] Siddharth Jain. Solving the Traveling Salesman Problem on the D-Wave Quantum Computer. *Frontiers in Physics*, 9, November 2021. Publisher: Frontiers.
- [9] Andrea Bonomi, Thomas De Min, Enrico Zardini, Enrico Blanzieri, Valter Cavecchia, and Davide Pastorello. Quantum Annealing Learning Search Implementations. *Quantum Information and Computation*, 22(3&4):181–208, February 2022.
- [10] Chen-Yu Liu, Hiromichi Matsuyama, Wei-hao Huang, and Yu Yamashiro. Quantum Local Search for Traveling Salesman Problem with Path-Slicing Strategy, July 2024.
- [11] Edward Farhi, Jeffrey Goldstone, and Sam Gutmann. A Quantum Approximate Optimization Algorithm, November 2014. arXiv:1411.4028 [quant-ph] <http://arxiv.org/abs/1411.4028>.

- [12] Oumayma Bouchmal, Bruno Cimoli, Ripalta Stabile, Juan Jose Vegas Olmos, and Idelfonso Tafur Monroy. Quantum Approximate Optimization Algorithm applied to multi-objective routing for large scale 6G networks. *Computer Networks*, 267:111345, July 2025.
- [13] Yue Ruan, Samuel Marsh, Xilin Xue, Zhihao Liu, and Jingbo Wang. The Quantum Approximate Algorithm for Solving Traveling Salesman Problem. *Computers, Materials & Continua*, 63(3):1237–1247, 2020. Publisher: Tech Science Press.
- [14] Yannis Spyridis, Athanasios Gkelias, and Vasileios Argyriou. Variational Quantum Approach for the Multiple Traveling Salesman Problem Optimisation. In *2023 19th International Conference on Distributed Computing in Smart Systems and the Internet of Things (DCOSS-IoT)*, pages 354–358, June 2023. ISSN: 2325-2944.
- [15] Simon Garhofer and Oliver Bringmann. Direct phase encoding in QAOA: Describing combinatorial optimization problems through binary decision variables, December 2024.
- [16] Andrew Lucas. Ising formulations of many NP problems. *Frontiers in Physics*, 2, 2014. arXiv:1302.5843 [cond-mat] <http://arxiv.org/abs/1302.5843>.
- [17] Vladimir Vargas-Calderón, Nicolas Parra-A, Herbert Vinck-Posada, and Fabio A. González. Many-Qudit representation for the Travelling Salesman Problem Optimisation. *Journal of the Physical Society of Japan*, 90(11):114002, November 2021.
- [18] Christopher D. B. Bentley, Samuel Marsh, André R. R. Carvalho, Philip Kilby, and Michael J. Biercuk. Quantum computing for transport optimization, June 2022.
- [19] Mehdi Ramezani, Sadegh Salami, Mehdi Shokhmkar, Morteza Moradi, and Alireza Bahrampour. Reducing the number of qubits from n^2 to $n \log_2(n)$ to solve the traveling salesman problem with quantum computers: A proposal for demonstrating quantum supremacy in the nisq era., February 2024.

- [20] Bence Bakó, Adam Glos, Ozlem Salehi, and Zoltán Zimborás. Prog-QAOA: Framework for resource-efficient quantum optimization through classical programs. *Quantum*, 9:1663, March 2025.
- [21] Sebastián V. Romero, Anne-Maria Visuri, Alejandro Gomez Cadavid, Anton Simen, Enrique Solano, and Narendra N. Hegade. Bias-field digitized counterdiabatic quantum algorithm for higher-order binary optimization. *Communications Physics*, 8(1):348, August 2025. Publisher: Nature Publishing Group.
- [22] Gan Zheng and Ioannis Krikidis. Constrained Higher-Order Binary Optimization for Wireless Communications Systems Using Ising Machines. *IEEE Transactions on Wireless Communications*, pages 1–1, 2025.
- [23] Daniel Goldsmith and Joe Day-Evans. Beyond QUBO and HOBO formulations, solving the Travelling Salesman Problem on a quantum boson sampler, June 2024. arXiv:2406.14252 [quant-ph] <http://arxiv.org/abs/2406.14252>.
- [24] Manuel Schnaus, Lilly Palackal, Benedikt Poggel, Xiomara Runge, Hans Ehm, Jeanette Miriam Lorenz, and Christian B. Mendl. Efficient Encodings of the Travelling Salesperson Problem for Variational Quantum Algorithms. In *2024 IEEE International Conference on Quantum Software (QSW)*, pages 81–87, July 2024.
- [25] Eric Bourreau, Gerard Fleury, and Philippe Lacommre. Indirect Quantum Approximate Optimization Algorithms: application to the TSP, November 2023. arXiv:2311.03294 [quant-ph] <http://arxiv.org/abs/2311.03294>.
- [26] Xujun Bai and Yun Shang. A quantum speedup algorithm for TSP based on quantum dynamic programming with very few qubits. *Theoretical Computer Science*, 1052:115423, October 2025.
- [27] Han Qi, Sihui Xiao, Zhuo Liu, Changqing Gong, and Abdullah Gani. Variational quantum algorithms: fundamental concepts, applications and challenges. *Quantum Information Processing*, 23(6):224, June 2024.
- [28] David Amaro, Matthias Rosenkranz, Nathan Fitzpatrick, Koji Hirano, and Mattia Fiorentini. A case study of variational quantum algorithms

for a job shop scheduling problem. *EPJ Quantum Technology*, 9(1):1–20, December 2022. Publisher: SpringerOpen.

- [29] Taylor L. Patti, Jean Kossaifi, Anima Anandkumar, and Susanne F. Yelin. Variational quantum optimization with multibasis encodings. *Physical Review Research*, 4(3):033142, August 2022. Publisher: American Physical Society.
- [30] Mateusz Słysz, Łukasz Grodzki, Piotr Rydlichowski, Dawid Siera, Krzysztof Kurowski, Grzegorz Waligóra, and Jan Węglarz. Solving combinatorial optimization and machine learning problems on hybrid near-term quantum photonic computers. *Future Generation Computer Systems*, 174:107934, January 2026.
- [31] Robert Sedgewick. Permutation Generation Methods. *ACM Comput. Surv.*, 9(2):137–164, June 1977.
- [32] Madhushree Das, Arindam Roy, Samir Maity, and Samarjit Kar. A Quantum-inspired Ant Colony Optimization for solving a sustainable four-dimensional traveling salesman problem under type-2 fuzzy variable. *Advanced Engineering Informatics*, 55:101816, January 2023.
- [33] Yida Li. Quantum Ant Colony Algorithm for Solving the Traveling Salesman Problem: A Theoretical and Practical Analysis. *Applied and Computational Engineering*, 110(1):175–181, November 2024.
- [34] Hao Li and Yue Ruan. Solving the Traveling Salesman Problem with Quantum Self-Attention Networks. In *2024 Cross Strait Radio Science and Wireless Technology Conference (CSRSWTC)*, pages 1–3, November 2024. ISSN: 2377-8512.
- [35] John J. Hopfield. Neural networks and physical systems with emergent collective computational abilities. *Proceedings of the National Academy of Sciences*, 79(8):2554–2558, 1982.
- [36] J. J. Hopfield and D. W. Tank. “Neural” computation of decisions in optimization problems. *Biological Cybernetics*, 52(3):141–152, July 1985.
- [37] Gang Feng and Christos Douligeris. *Using Hopfield networks to solve traveling salesman problems based on stable state analysis technique*, volume 6. IEEE, February 2000. Journal Abbreviation: Proceedings of the

International Joint Conference on Neural Networks Pages: 526 vol.6
Publication Title: Proceedings of the International Joint Conference on
Neural Networks.

- [38] Paulo Henrique Siqueira, Sergio Scheer, and Maria Teresinha Arns Steiner. A Recurrent Neural Network to Traveling Salesman Problem. In Federico Greco, editor, *Traveling Salesman Problem*. IntechOpen, Rijeka, 2008. Section: 7.
- [39] Bert F. J. La Maire and Valeri M. Mladenov. Comparison of neural networks for solving the travelling salesman problem. In *11th Symposium on Neural Network Applications in Electrical Engineering*, pages 21–24, September 2012.
- [40] Martin Larocca, Supanut Thanasilp, Samson Wang, Kunal Sharma, Jacob Biamonte, Patrick J. Coles, Lukasz Cincio, Jarrod R. McClean, Zoë Holmes, and M. Cerezo. Barren Plateaus in Variational Quantum Computing. *Nature Reviews Physics*, 7(4):174–189, March 2025.
- [41] M. Cerezo, Martin Larocca, Diego García-Martín, N. L. Diaz, Paolo Braccia, Enrico Fontana, Manuel S. Rudolph, Pablo Bermejo, Aroosa Ijaz, Supanut Thanasilp, Eric R. Anschuetz, and Zoë Holmes. Does provable absence of barren plateaus imply classical simulability? Or, why we need to rethink variational quantum computing. *Nature Communications* 16, 7907, 2025.
- [42] Reuben Tate and Stephan Eidenbenz. Theoretical Approximation Ratios for Warm-Started QAOA on 3-Regular Max-Cut Instances at Depth p=1. *Theoretical Computer Science*, page 115571, October 2025.
- [43] Frederic Sauvage, Sukin Sim, Alexander A. Kunitsa, William A. Simon, Marta Mauri, and Alejandro Perdomo-Ortiz. FLIP: A flexible initializer for arbitrarily-sized parametrized quantum circuits, May 2021. arXiv:2103.08572 [quant-ph] <http://arxiv.org/abs/2103.08572>.
- [44] Belozerova Polina, Shangareev Arthur, Zotov Yuriy, Yung Manhong, and lv Dingshun. Hot-Start Optimization for Variational Quantum Eigensolver, April 2021. arXiv:2104.15001 [quant-ph] <http://arxiv.org/abs/2104.15001>.

- [45] Erik Recio-Armengol, Shahnawaz Ahmed, and Joseph Bowles. Train on classical, deploy on quantum: scaling generative quantum machine learning to a thousand qubits, March 2025. arXiv:2503.02934 [quant-ph] <http://arxiv.org/abs/2503.02934>.
- [46] Adam Paszke, Sam Gross, Francisco Massa, Adam Lerer, James Bradbury, Gregory Chanan, Trevor Killeen, Zeming Lin, Natalia Gimelshein, Luca Antiga, Alban Desmaison, Andreas Köpf, Edward Yang, Zach DeVito, Martin Raison, Alykhan Tejani, Sasank Chilamkurthy, Benoit Steiner, Lu Fang, Junjie Bai, and Soumith Chintala. PyTorch: An Imperative Style, High-Performance Deep Learning Library, December 2019. arXiv:1912.01703 [cs] <http://arxiv.org/abs/1912.01703>.
- [47] Adam Paszke et al. torchviz - visualize pytorch execution graphs. <https://github.com/szagoruyko/torchviz>, 2019. Accessed: 2025-04-19.
- [48] Kosuke Mitarai, Makoto Negoro, Masahiro Kitagawa, and Keisuke Fujii. Quantum Circuit Learning. *Physical Review A*, 98(3):032309, September 2018.
- [49] Maria Schuld, Ville Bergholm, Christian Gogolin, Josh Izaac, and Nathan Killoran. Evaluating analytic gradients on quantum hardware. *Physical Review A*, 99(3):032331, March 2019.
- [50] J. Spall. A Stochastic Approximation Technique for Generating Maximum Likelihood Parameter Estimates. *American Control Conference*, 1987.
- [51] IBM Quantum. Compute resources, 2025. Available from: <https://quantum.cloud.ibm.com/quantum.cloud.ibm.com>. Accessed 6 July 2025.
- [52] Gerhard Reinelt. TSPLIB—A Traveling Salesman Problem Library. *ORSA Journal on Computing*, 3(4):376–384, November 1991. Publisher: ORSA.
- [53] Daniel Goldsmith. Github repository: goldsmdn/TSP_vqc: Travelling Salesman problem with a variational quantum circuit, 2025. https://github.com/goldsmdn/TSP_VQC.

- [54] Ali Javadi-Abhari, Matthew Treinish, Kevin Krsulich, Christopher J. Wood, Jake Lishman, Julien Gacon, Simon Martiel, Paul D. Nation, Lev S. Bishop, Andrew W. Cross, Blake R. Johnson, and Jay M. Gambetta. Quantum computing with Qiskit, June 2024. arXiv:2405.08810 [quant-ph] <http://arxiv.org/abs/2405.08810>.
- [55] Ian Goodfellow, Yoshua Bengio, and Aaron Courville. *Deep Learning*. MIT Press, 2016. <http://www.deeplearningbook.org>.
- [56] Anas Skalli, Satoshi Sunada, Mirko Goldmann, Marcin Gębski, Stephan Reitzenstein, James A. Lott, Tomasz Czyszanowski, and Daniel Brunner. Model-free front-to-end training of a large high performance laser neural network, March 2025. arXiv:2503.16943 [cs] <http://arxiv.org/abs/2503.16943>.
- [57] Christos H Papdimitriou and Kenneth Steiglitz. *Combinatorial Optimisation: Algorithms and Complexity*. Dover, 1998.
- [58] Vincent Sitzmann, Julien N. P. Martel, Alexander W. Bergman, David B. Lindell, and Gordon Wetzstein. Implicit Neural Representations with Periodic Activation Functions, June 2020. arXiv:2006.09661 [cs] <https://arxiv.org/abs/2006.09661>.
- [59] Kaiming He, Xiangyu Zhang, Shaoqing Ren, and Jian Sun. Delving Deep into Rectifiers: Surpassing Human-Level Performance on ImageNet Classification, February 2015. arXiv:1502.01852 [cs] <https://arxiv.org/abs/1502.01852>.
- [60] A. Shamshad, M. A. Bawadi, W. M. A. Wan Hussin, T. A. Majid, and S. A. M. Sanusi. First and second order Markov chain models for synthetic generation of wind speed time series. *Energy*, 30(5):693–708, April 2005.
- [61] Elicit. Elicit: The AI research assistant, 2025. <https://elicit.com>.
- [62] OpenAI. ChatGPT, 2025. Accessed: <https://chat.openai.com/chat>.

8 Declaration of generative AI and AI-assisted technologies in the manuscript preparation process

During the preparation of this work the authors used Elicit [61] in order to validate the original review of the literature, ChatGPT [62] to research key concepts, and Writefull to improve the readability of the article. After using these tools, the authors reviewed and edited the content as needed and take full responsibility for the content of the published article.

A Appendix - Parameter settings

Parameter	VQA/ML	Default	Notes
Iterations (epochs)	VQA + ML	250	
Formulation	VQA + ML	Original	Section 4.4.5
Warm start	VQA + ML	False	Section 4.4.6
ML input vector no warm start	ML	Zeros	Section B.3
Gray	VQA + ML	False	Section 4.4.8
Circuit	VQA	2	Section B.1
Layers for ML	ML	4	Section B.3
shots	VQA	1024	
Number of input vectors (shots)	ML	64	Section B.3
Gradient type	VQA	SPSA	Section 4.4.2
Gradient type	ML	SGD	Section 4.4.3
Slice	VQA	0.8	Section 4.4.4
Slice	ML	1.0	Section 4.4.4
A	VQA SPSA	25	Section 4.4.2
c	VQA SPSA	$\pi/10 = 0.314$	Section 4.4.2
α	VQA SPSA	0.602	Section 4.4.2
Learning rate (η)	VQA SPSA	0.1	Section 4.4.2
γ	VQA SPSA	0.101	Section 4.4.2
Learning rate (η)	VQA Parameter Shift	0.1	Section 4.4.2
s	VQA Parameter shift	0.5	Section 4.4.2
σ	ML	0.05	Section 4.4.3
LR (η)	ML SGD	2×10^{-5}	Section 4.4.3
Momentum β	ML SGD	0.8	Section 4.4.3
Weight decay λ	ML SGD	0.0006	Section 4.4.3
LR (η)	ML Adam	0.001	Section 4.4.3
Momentum β_1	ML Adam	0.9	Section 4.4.3
Weight decay λ	ML Adam	0.0032	Section 4.4.3

Table 3: Default parameters used

B Appendix - Detailed results

B.1 Qiskit simulation of quantum circuit model

The results for the five quantum circuit models studied, with default parameters, are presented in Table 4. Detailed results for twelve locations are shown in Table 5. Circuit 1 appears to perform slightly better than the other circuits and the Monte Carlo method, however this result is not statistically significant. Circuit 3 and 4 have only one parameter per qubit, and so there are fewer gradients taken, which is why fewer binary strings are sampled. The circuits without entanglement performs worse than the other circuits, however, this result is not statistical significant.

Locs	Binary Vars	Circuit 1	Circuit 2	Circuit 3	Circuit 4	Circuit 5	Monte Carlo	Min. runs
4	3	100.0 \pm 0.0	9					
5	5	100.0 \pm 0.0	9					
6	8	100.0 \pm 0.0	100.0 \pm 0.0	98.3 \pm 1.4	99.7 \pm 0.3	100.0 \pm 0.0	100.0 \pm 0.0	9
7	11	100.0 \pm 0.0	100.0 \pm 0.0	99.7 \pm 0.3	97.8 \pm 1.5	100.0 \pm 0.0	100.0 \pm 0.0	9
8	14	100.0 \pm 0.0	100.0 \pm 0.0	99.6 \pm 0.3	96.8 \pm 1.5	100.0 \pm 0.0	100.0 \pm 0.0	9
9	17	98.9 \pm 0.8	100.0 \pm 0.0	97.9 \pm 1.2	92.7 \pm 1.8	98.8 \pm 0.9	100.0 \pm 0.0	9
10	21	98.4 \pm 0.8	99.5 \pm 0.4	96.0 \pm 1.6	92.7 \pm 2.1	98.7 \pm 0.1	100.0 \pm 0.0	9
11	25	98.9 \pm 0.2	99.5 \pm 0.3	97.6 \pm 1.0	96.0 \pm 1.0	99.7 \pm 0.1	99.6 \pm 0.5	7
12	29	95.4 \pm 1.2	93.5 \pm 0.8	92.9 \pm 1.6	88.3 \pm 2.5	90.5 \pm 1.9	94.0 \pm 0.1	7
Overall		99.1 \pm 0.3	99.2 \pm 0.2	98.0 \pm 0.8	96.0 \pm 1.2	98.6 \pm 0.4	99.3 \pm 0.1	

Table 4: Table of VQA solution quality for different numbers of locations and different circuits.

Model	Solution Quality	Params. per qubits	Av. bit strings sampled
Circuit 1	95.4 ± 1.2	2	1,003,353
Circuit 2	93.5 ± 0.8	2	1,011,155
Circuit 3	92.9 ± 1.6	1	651,055
Circuit 4	88.3 ± 2.5	1	649,284
Circuit 5	90.5 ± 1.9	2	992,704
Monte Carlo	94.0 ± 0.1	n/a	1,025,235
Greedy classical	77.1	n/a	n/a

Table 5: The summary of VQA solution quality in percent for the five circuits tested show that Circuit 1 and Circuit 2 have slightly better solution quality. No circuits beat the Monte Carlo simulation

B.2 Ablation results

Locs.	Fact.	Non Fact.
4	100.0	100.0
5	100.0	100.0
6	100.0	100.0
7	100.0	100.0
8	100.0	100.0
9	100.0	100.0
10	99.1	99.4
11	99.2	99.5
12	91.4	93.5
Overall	98.9	99.2

(a) Average solution quality for the factorial and non-factorial formulation in the **VQA** model.

Locs.	Fact.	Non Fact.
4	100.0	100.0
5	100.0	100.0
6	99.3	99.5
7	95.5	88.2
8	81.9	89.7
9	85.0	82.1
10	76.9	72.0
11	87.4	88.5
12	68.8	68.1
15	69.9	65.6
17	72.6	68.9
Overall	85.2	83.9

(b) Average solution quality for the factorial and non-factorial formulation in the **classical ML** model.

Table 6: There is little difference between the solution quality in percent for the factorial and non-factorial formulation in the ML and VQA model with different number of locations.

Locations	Non-factorial Qubits	Factorial Qubits
5	5	7
10	21	22
15	41	41
20	64	62
25	89	84
30	114	108
35	141	133
40	171	160
45	201	187
50	231	215
55	261	243
60	291	273

Table 7: Qubits required for different location sizes for different network sizes for the factorial and non-factorial formulation.

Locations	Without warm start	With warm start
4	100.0	100.0
5	100.0	100.0
6	98.3	88.7
7	88.6	100.0
8	90.9	94.6
9	83.3	100.0
10	75.8	90.5
11	89.1	93.0
12	66.2	78.8
15	66.4	70.4
17	70.2	70.7
26	94.1	78.0
42	100.0	77.7
48	9.3	9.4
Overall	80.9	82.3

Table 8: There is little difference in average solution quality in percent with and without warm start for the **classical ML** model with different location numbers

Locations	Without warm start	With warm start
4	100.0	100.0
5	100.0	100.0
6	100.0	100.0
7	100.0	100.0
8	100.0	100.0
9	100.0	100.0
10	99.4	98.9
11	99.5	100.0
12	93.5	93.3
Overall	99.2	99.1

Table 9: There is little difference in average solution quality in percent with and without warm start for the **VQA** model with different location numbers

Locations	Qubits	Best dist.	Warm start dist.	Warm start sol. qual.	Lowest hamming dist.
4	3	21.0	21.0	100.0	0
5	5	19.0	21.0	90.5	2
6	8	241.0	279.6	86.2	5
7	11	276.2	314.8	87.7	5
8	14	277.2	315.8	87.8	8
9	17	286.7	339.8	84.4	9
10	21	290.2	312.3	92.9	8
11	25	253.0	299.0	84.6	9
12	29	297.2	385.5	77.1	10

Table 10: Table showing that the Hamming distance between the warm start and optimum cycle is relatively large. The table shows distances, warm start solution quality in percent, and Hamming distances for various locations and qubits.

Location	No Gray codes	Gray codes
4	100.0	100.0
5	100.0	100.0
6	100.0	100.0
7	100.0	100.0
8	100.0	100.0
9	100.0	99.4
10	99.4	98.5
11	99.5	98.8
12	93.5	96.7
Overall	99.2	99.3

(a) Solution quality with and without Gray codes for the **VQA** model.

Location	No Gray codes	Gray codes
4	100.0	100.0
5	100.0	98.1
6	99.5	100.0
7	88.2	98.9
8	89.7	80.6
9	82.1	78.4
10	72.0	72.0
11	88.5	89.3
12	68.1	70.4
15	65.6	67.1
17	68.9	71.9
26	94.1	93.5
42	100.0	100.0
48	9.4	9.6
Overall	80.4	80.7

(b) Solution quality with and without Gray codes for the **Classsical ML** model.

Table 11: There is little difference between the solution quality in percent with and without Gray codes for the **VQA classical ML** with different number of locations.

B.3 Classical Machine learning model

The average error for the classical machine model, with optimal parameters, by location and number of layers is plotted in Figure 10 in Appendix C and the corresponding solution quality is provided in Table 12. The results show that the number of layers has little impact on the final quality of the solution.

The number of input vectors were varied for each epoch for different numbers of locations. The summary results are plotted in Figure 11, shown in summary in Table 13 with detailed results in Table 16. Although the quality of the solution increases with the number of input vectors, so does the run time, which varies approximately linearly with the number of input vectors.

Locations	1 layer	2 layers	3 layers	4 layers
4	100.0	100.0	100.0	100.0
5	100.0	100.0	100.0	100.0
6	94.0	94.0	100.0	99.5
7	89.7	89.0	89.7	88.2
8	99.8	83.3	97.1	89.7
9	83.3	92.1	81.5	82.1
10	81.1	77.1	74.1	72.0
11	89.4	87.5	93.4	88.5
12	64.8	58.8	63.5	68.1
15	66.1	69.0	68.8	65.6
17	76.6	70.0	71.7	68.9
26	94.1	94.1	94.1	94.1
42	100.0	100.0	100.0	100.0
48	9.3	9.2	8.9	9.4
Overall	82.0	80.3	81.6	80.4

Table 12: There is little difference between the solution quality, in percent, for the ML models, with 1, 2, 3 and 4 layers with networks of different number of locations. No sample error is estimated as most combinations were only run once.

As discussed above, using more shots improves the fraction of the solution space investigated, and this might explain the increase in solution quality. 64 input vectors per epoch were used for hyper-parameter optimisation as a good compromise between solution quality and execution time. The results quoted in the general result summary in Section 4.3 are for 1,024 input vectors. The warm start results in Section 4.4.6 in Appendix C and the impact of the ML layers above are based on runs with 64 input vectors.

No. of input vectors	Solution found on iteration (av.)	Av solution quality	Av. Execution time (secs)
4	79.3	80.1	42
8	49.1	78.0	84
16	41.2	78.6	166
32	32.2	82.3	331
64	37.9	81.2	658
128	41.2	85.0	1,346
256	49.4	87.2	2,854
512	58.8	88.1	8,090
1,024	72.3	92.3	10,082

Table 13: The overall average solution quality in percent and elapsed time increases as the number of input binary vectors (mini-batches) increases for the classical machine model, at the expense of enhanced execution time.

The input vectors were initialised to values of 0, or 0.5. Detailed results are shown for 64 and 256 input vectors, respectively, in Tables 14 and 15 showing that although the solution quality is slightly better for initialisations with 0.5 with 64 input vectors, this result does generalise to 256 input vectors.

Locations	Input vector with zeros	Input vector with 0.5
4	100.0 ± 0.0	100.0 ± 0.0
5	100.0 ± 0.0	100.0 ± 0.0
6	99.3 ± 0.7	96.3 ± 2.5
7	87.9 ± 1.2	93.1 ± 2.8
8	93.9 ± 3.8	94.5 ± 3.5
9	81.8 ± 2.8	91.5 ± 2.9
10	71.9 ± 2.7	83.0 ± 3.0
11	88.2 ± 0.4	92.8 ± 0.3
12	70.4 ± 4.5	80.9 ± 0.7
15	67.9 ± 1.7	70.0 ± 0.8
17	71.5 ± 0.6	72.1 ± 1.8
26	94.1 ± 0.9	92.5 ± 0.7
42	100.0 ± 0.0	100.0 ± 0.0
48	9.4 ± 0.1	9.2 ± 0.0
Overall	81.2 ± 1.3	84.0 ± 1.4

Table 14: There is little difference in average solution quality in percent with different initialisation values with 64 input vectors for different network sizes

Locations	Input vector with zeros	Input vector with 0.5
4	100.0 ± 0.0	100.0 ± 0.0
5	100.0 ± 0.0	100.0 ± 0.0
6	100.0 ± 0.0	100.0 ± 0.0
7	100.0 ± 0.0	100.0 ± 0.0
8	100.0 ± 0.0	100.0 ± 0.0
9	99.0 ± 0.9	100.0 ± 0.0
10	96.6 ± 0.6	91.5 ± 0.6
11	91.9 ± 0.9	98.4 ± 0.4
12	84.4 ± 2.3	85.2 ± 0.6
15	71.3 ± 0.4	70.1 ± 1.2
17	77.3 ± 3.1	74.2 ± 2.1
26	89.7 ± 0.9	90.6 ± 0.0
42	100.0 ± 0.0	100.0 ± 0.0
48	10.2 ± 0.2	9.7 ± 0.0
Overall	87.2 ± 0.7	87.1 ± 0.4

Table 15: There is no significant difference between the average solution quality in percent for different initialisation values with 256 input vectors and different network sizes

loc/inpu	2	4	8	16	32	64	128	256	512	1,024
4	100.0	100.0	100.0	100.0	100.0	100.0	100.0	100.0	100.0	100.0
5	100.0	100.0	100.0	100.0	100.0	100.0	100.0	100.0	100.0	100.0
6	94.0	94.0	94.0	94.0	100.0	100.0	100.0	100.0	100.0	100.0
7	100.0	89.7	89.7	87.7	89.0	83.2	89.0	100.0	100.0	100.0
8	82.4	83.5	82.7	83.3	100.0	87.0	100.0	100.0	100.0	100.0
9	92.1	83.3	74.0	81.4	92.1	88.9	100.0	99.8	100.0	100.0
10	64.3	72.9	61.1	73.3	73.7	65.1	88.3	97.3	100.0	97.5
11	86.3	87.5	87.5	90.7	87.5	88.5	87.5	92.0	98.8	98.7
12	65.1	65.8	58.8	63.3	70.0	81.9	78.7	88.1	83.5	90.7
15	59.5	70.8	73.9	65.4	65.5	61.8	73.1	71.9	73.3	74.7
17	58.3	72.4	72.0	58.3	71.8	73.0	72.6	74.6	77.9	82.7
26	91.5	92.7	89.0	94.1	94.1	94.1	90.6	90.6	90.6	90.6
42	100.0	100.0	100.0	100.0	100.0	100.0	100.0	100.0	100.0	100.0
48	9.2	8.6	9.0	8.8	8.9	9.5	9.5	10.1	9.5	10.3

Table 16: The solution quality in percent increases as the number of input vectors (mini-batches) increases for the classical machine model.

B.4 Caching

Locations	Distinct cycles through network	Average ML cache calls ($H + M$)	Average VQA cache calls ($H + M$)	ML coverage \mathcal{C}	VQA coverage \mathcal{C}
4	3	1,028,096	7,947	> 1	> 1
5	12	1,542,144	19,661	> 1	> 1
6	60	2,313,216	94,151	> 1	> 1
7	360	3,084,288	187,519	> 1	> 1
8	2,520	3,855,360	549,048	> 1	> 1
9	20,160	4,626,432	681,525	> 1	> 1
10	181,440	5,654,528	896,274	> 1	> 1
11	1,814,400	6,682,624	957,261	> 1	0.520
12	19,958,400	7,710,720	1,011,155	0.386	0.050
15	4.359e+10	1.080e+07	n/a	2.477e-04	n/a
17	1.046e+13	1.285e+07	n/a	1.228e-06	n/a
26	7.756e+24	2.442e+07	n/a	3.148e-18	n/a
42	1.673e+49	4.729e+07	n/a	2.827e-42	n/a
48	1.293e+59	5.655e+07	n/a	4.373e-52	n/a

Table 17: Number of distinct cycles compared to cache calls. For network sizes of less than 10 locations, more bits strings were sampled than distinct cycles. However, for larger networks the number of strings sampled is only a small fraction of the cycles through the network.

C Appendix - Supplementary figures

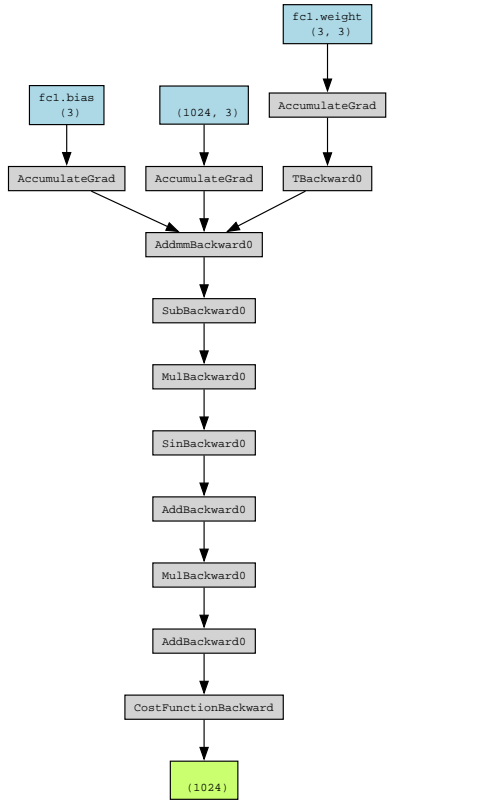


Figure 8: Computation graph for the classical machine learning model with one layers produced with Torchviz.

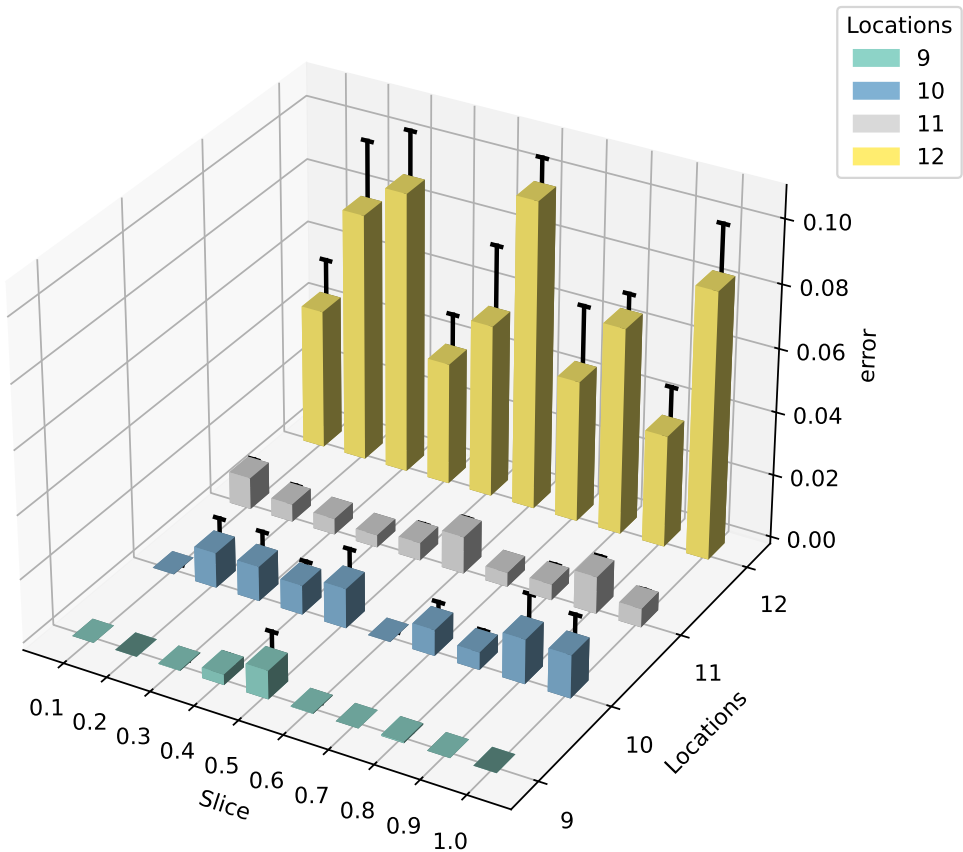


Figure 9: Average VQA error by slicing for different location rates. Results for fewer than nine locations are omitted, as the corresponding error rates are very low and not clearly visible in the plot.

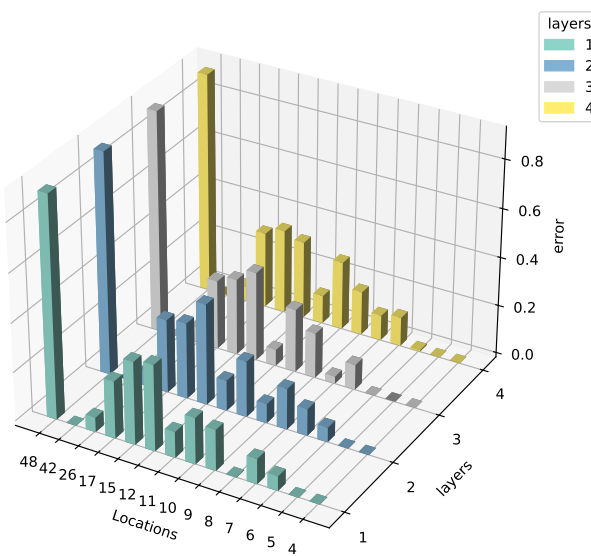


Figure 10: Error rates in the classical machine learning models for different locations and layer, showing the number of layers makes little difference.

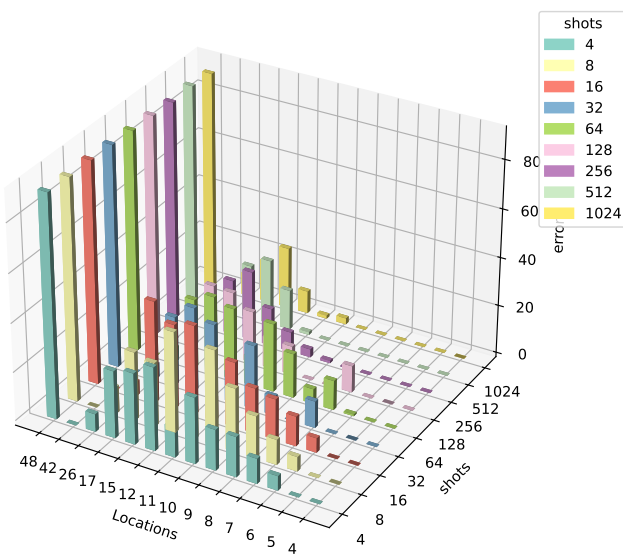


Figure 11: Solution error in %age for ML with the number of binary input vectors (shots, or mini-batches) against the number of locations, showing that the error reduce as the numbers of the binary input vectors increase